Chaotic Gas Accretion by Black Holes Embedded in AGN Disks as Cause of Low-spin Signatures in Gravitational Wave Events

Yixian Chen (yc9993@princeton.edu)
Princeton University https://orcid.org/0000-0003-3792-2888
Douglas Lin
University of California https://orcid.org/0000-0001-5466-4628

Article

Keywords:

Posted Date: July 15th, 2022

DOI: https://doi.org/10.21203/rs.3.rs-1860933/v1

Chaotic Gas Accretion by Black Holes Embedded in AGN Disks as Cause of Low-spin Signatures in Gravitational Wave Events

Yi-Xian Chen[1,*] **and Douglas N. C. Lin**[2,3]

[1]Department of Astrophysical Sciences, Princeton University, USA
[2]Department of Astronomy & Astrophysics, University of California, Santa Cruz, CA 95064, USA
[3]Institute for Advanced Studies, Tsinghua University, Beijing 100084, China
[*]yc9993@princeton.edu

ABSTRACT

Accretion disks around super-massive black holes (SMBH) not only power active galactic nuclei (AGNs) but also host single and binary embedded stellar-mass black holes (EBHs). The merger of these EBHs provides a promising mechanism for the excitation of some gravitational wave events observed by LIGO-Virgo. In addition to their mass and mass-ratio distribution, their hitherto enigmatic small spin-parameters ($\chi_{\rm eff}$) carry important clues and stringent constraints on their formation channels and evolutionary pathways. Here we show that, after each coalescence, the typical rapid spin of the merged EBHs is suppressed by their subsequent accretion of gas from a turbulent environment, due to its ability to randomize the flow's spin orientation with respect to that of the EBHs on an eddy-turnover timescale. This theory provides supporting evidence for the prolificacy of EBH mergers and suggests that their mass growth is dominated by gas accretion rather than their coalescence in AGN disks. In addition to their contributions to the mass and $\chi_{\rm eff}$ distribution observed by LIGO-Virgo, EBHs' gas accretion also provides auxiliary powers to the heating of the global disk in AGNs.

Direct observation of the center of our milky way[1–4], as well as abundant tidal disruption event samples[5–7] suggest that stellar clusters commonly exist around super-massive black holes (SMBHs)[8]. In active galactic nuclei (AGNs), the cluster stars may be captured into circularized orbits on the SMBH accretion disk midplane through resonance coupling and gas drag during disk passage[9–11]. Embedded stars may also form *in situ* from gravitational instability[12–16] and migrate throughout AGN disks. Due to the rapid accretion of disk material, they evolve quickly to become massive stars[17] and then undergo supernova or gravitational collapse, leaving behind not only ejecta that might account for metallicity abundances in AGNs[18,19], but also embedded stellar mass black holes (EBHs). Binary stellar-mass black holes (BBHs) may form and harden through the accumulation of stand-alone EBHs at migration traps, as well as their single-single dynamical encounters, and potentially produce gravitational waves (GW) that contribute to some LIGO-Virgo events[20–24]. In particular, BBH mergers in an AGN disk may shock-heat the surrounding accretion flow and generate optical/UV flares, an electromagnetic counterpart that could differentiate them from other merger channels[25].

The coalescence of two comparable-mass EBHs generally leads to a merged product with a combined mass $M_\star$ and large spin angular momentum $J_\star$[26]. In a laminar global AGN disk, EBHs with circularized orbits around the SMBH can gain spin angular momentum between merger events through gas accretion from their local circum-stellar disks (CSDs), and quickly become aligned with each other (prograde to the disk rotation). The coalescence of such EBHs also favors high-spin merger events. However, the projection of the mass-weighted spin-angular-momentum of individual EBHs in the BBHs' orbital angular momentum direction ($\chi_{\rm eff}$), inferred from the observed GW events, prefers low values[27]. This distribution suggests low natal EBH spins or random directions between the binary orbital angular momentum and the EBHs' individual spins[28]. While dynamical encounters between BBHs/EBHs and other stars can tilt their orbital planes significantly away from the disk plane[23], EBHs or BBHs with non-negligible eccentricity are also surrounded by CSDs with retrograde spins[29] which introduces misalignment between spin axes of merging EBHs, as possible solutions to this paradox. En route potential paths of BBHs' migration, evection and eviction resonances between their precession and orbital frequencies can excite eccentricity in BBHs with nearly co-planar and highly inclined orbits whereas spin-orbit resonances can also modify BBHs' obliquity[30].

While fore-mentioned mechanisms rely on misalignment/counter-alignment between EBH populations to produce low-$\chi_{\rm eff}$ events, they pose no constraint on the growth of individual EBH spins. Magneto-rotational and gravitational instabilities (MRI and GI), both common in AGN accretion disks[14], excite turbulence with locally chaotic eddies[13,31]. In this letter, we show that that EBHs' accretion from these eddies provides an alternative and novel mechanism to robustly reduce the dimensionless

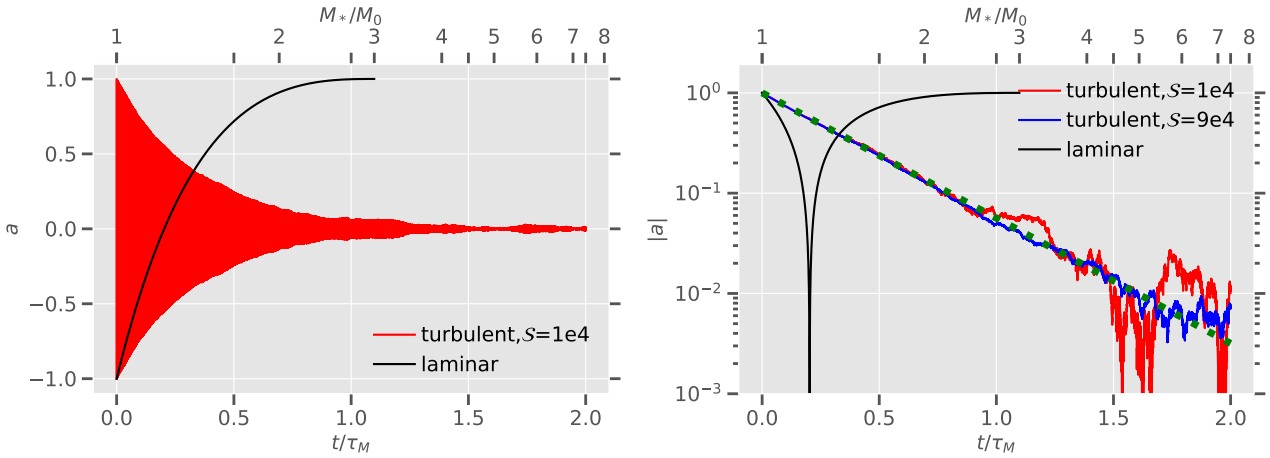

Figure 1. Left panel: Evolution of EBH spin a with sign determined with respect to CSD spin for the laminar case (fixed CSD spin direction, black line), and turbulent case with $\mathcal{S} = 10^4$ (red line). In the turbulent case, the CSD spin changes discontinuously every accretion episode so a shifts between positive and negative values with a trend of decaying in magnitude; Right panel: Evolution of $|a|$ in these cases, with an additional $\mathcal{S} = 9 \times 10^4$ case shown in blue solid line. The green dotted line shows analytical prediction for the initial spin-down phase, before the spin magnitude becomes comparable to $\mathcal{S}^{-0.5}$.

spin parameter $a = cJ_\star/GM_\star^2$ of individual EBHs before they capture their binary companions. In the EBH-centric coordinates, the inclination θ between CSD spin vector $\mathbf{J_d}$ and EBH spin vector $\mathbf{J}_\star$ is frequently randomized, and the growth of EBH's spin occurs through a series of short and independent accretion episodes. The final characteristic magnitude of EBHs' spin is limited by a random walk (RW) factor on the order of $a_{RW} \sim \mathcal{S}^{-0.5}$, where $\mathcal{S}(\gg 1)$ is the number of CSD spin-reorientation episodes during each Eddington mass doubling timescale. Moreover, the spin axes distribution also becomes isotropic. For typical turbulence in AGN disks, the characteristic turbulence-coherence (eddy-turnover) timescale is the local dynamical timescale, which gives $\mathcal{S} \sim 10^4$ (see Methods). A final spin distribution with low magnitude and isotropic direction implies a general low-$\chi_{\rm eff}$ distribution in subsequent merger events.

The left panel of Figure 1 shows two exemplary individual cases of EBH spin a evolution. By convention, the sign of a is determined *relative to the local CSD flow*[23,32], or explicitly, $a = |a|\mathrm{sign}(\cos\theta) = |a|\mathrm{sign}(\mathbf{J_d}\cdot\mathbf{J}_\star)$. In a laminar AGN disk, a steady-state CSD flow is either prograde or retrograde with respect to the absolute global disk rotation[29], and EBH spin will monotonically grow towards this preferred direction. The solid black line shows how an initially counter-aligned $a = -1$ EBH would grow its spin towards the CSD rotation axis, with mass increasing exponentially on the doubling timescale $\tau_{\rm M} = \tau_{\rm Sal}\eta_\star$ through Eddington-limited accretion, where $\tau_{\rm Sal}$ is the Salpeter timescale[33] and $\eta_\star$ is the EBH accretion efficiency. In this ideal reference case, we assume initial spin axis is counter-aligned with CSD spin, and in time $\theta = \pi$ would discontinuously jump to $\theta = 0$ as a crosses over to positive, since for $\theta = \pi, 0$ there is no Lense-Thirring (LT) precession torque to change θ continuously (see Methods). On this "fundamental track", the EBH can at most grow its mass up to $3M_0$ during this spin accretion process, where M_0 is the initial mass, as it reaches asymptotic limit $a \simeq 1$ after a timescale of $\tau_{\rm M}\ln(3)$. EBHs born with spin larger than -1 starts somewhere middle on this same track but the final spins all converge towards 1.

The red line in left panel of Figure 1 shows evolution of a in a fiducial turbulent case with $\mathcal{S} = 10^4$. The initial magnitude of the spin is $|a| = 1$, but at the start of every accretion episode with constant duration $\tau_{\rm M}/\mathcal{S} = \tau_{\rm Sal}\eta_\star/\mathcal{S}$, the orientation of CSD spin is randomized with respect to the current EBH spin, and we take account of LT torque in the evolution of θ during every episode. Although a, by definition (see Methods), oscillates between positive and negative values due to the sporadic shift of CSD spin, through plotting the evolution of $|a|$ in the right panel of Figure 1 in logarithmic scale, we can more clearly see a continuous change in the spin magnitude. We found in the turbulent case, the typical value of $|a|$ first evolves as an exponential decay due to the intrinsic asymmetry between spin-up and spin-down, but after some typical spin-down timescale τ_d comparable to $\tau_{\rm M}$, random fluctuations around $a = 0$ due to accretion of individual cycles dominate, and characteristic values fluctuate around the random-walk dispersion $a_{RW} \sim \mathcal{S}^{-0.5}$. We also tested with $\mathcal{S} = 9 \times 10^4$ (right panel, blue line), in which case the random walk factor is smaller, and a longer decay timescale τ_d is needed for the initial spin to decay below this factor. The green dotted line shows analytical prediction $|a| \approx \exp(-2.876t/\tau_{\rm M})$, which could very well describe the initial spin-down phase. The derivation of this prescription as well as expression $\tau_d \approx \tau_M \ln\mathcal{S}/5.752$ are elaborated in the Appendix.

In the left panel of Figure 2 we show evolution of average dispersion $\langle a^2\rangle$ for a population of 10^3 EBHs, starting from a uniform distribution of a between -1 and 1. The root mean square of the spin converges towards an asymptotic value of

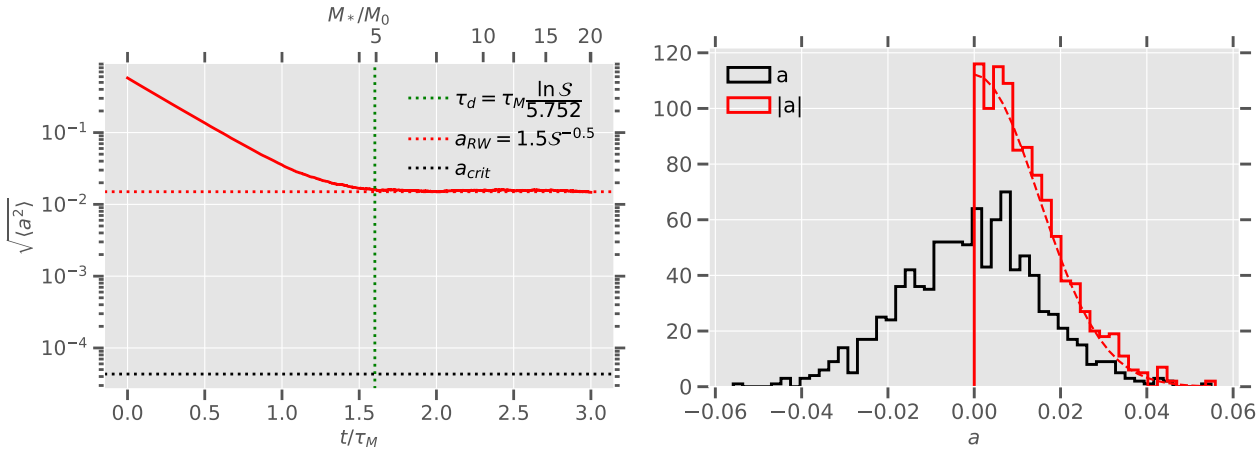

Figure 2. Spin evolution of a population of 10^3 EBHs with $\mathcal{S} = 10^4$. Left panel: the root-mean-square of spin parameter, evolving with time, shown in red solid line. The decay time (green dotted line) serves as an accurate estimate of the time where initial $\sqrt{\langle a^2 \rangle} = 1/\sqrt{3}$ (for uniform distribution) decays to the random walk factor a_{RW} (red dotted line), which is much larger than the critical spin (black dotted line) required for systematic spin-up by LT torque; Right panel: The histogram of a and $|a|$ after 3 $\tau_{\rm M}$, reaching a semi-steady state. The distribution of $|a|$ can very well be approximated by half a Gaussian with standard deviation a_{RW}.

$a_{RW} \approx 1.5\mathcal{S}^{-0.5}$ (red dotted horizontal line), and it does not grow subsequently as it would have in a pure RW. This outcome is due to the competing effect of spin down and RW. With $|a| \approx a_{RW}$, the spin down effect that reduces $|a|$ has stricken an equilibrium with RW diffusion that tends to expand $|a|$. The decay time τ_d is shown as the green dotted line, which serves as an estimate of the time of transition from initial spin-down-dominated phase to a RW-dominated phase on a population level, since it reflects the slowest possible spin-down timescale of any EBH within this population. The critical spin a_{crit} (black dotted line) below which LT effect becomes important is a sensitive function of $\mathcal{S}$ (see Figure 3 and Methods). Since the characteristic value of $|a|$ never gets below $a_{RW} \gg a_{crit}$, LT torque does not play a significant role in this evolution process.

In the right panel of Figure 2, we show the histogram for a and $|a|$. Note that due to the slight asymmetry between spin up and spin down with respect to $\mathbf{J_d}$ (spin down is more efficient), the PDF of a has a mean value slightly shifted towards the positive. However by formulation, the $\mathbf{J_d}$ vector distribution is also isotropic, therefore the distribution of spin *projection* $|a|\text{sign}(\mathbf{J_d} \cdot \mathbf{z})$ with respect to any reference absolute vector $\mathbf{z}$ would essentially be a symmetrically expanded version of the magnitude $|a|$ distribution. We show that the $|a|$ histogram can be approximated very well by Gaussians with dispersion $1.5\mathcal{S}^{-0.5}$ (dashed red line).

In Figure 3 we plot $\sqrt{\langle a^2 \rangle}$ for different populations after $3\tau_M$ with a range of $\mathcal{S}$. Provided $\mathcal{S} > 100$, $\sqrt{\langle a^2 \rangle} \simeq 1.5\mathcal{S}^{-0.5}$ very accurately. For the LT-free models (e.g. θ does not evolve during each spin-reorientation episode, see Methods for details), $\sqrt{\langle a^2 \rangle}$ completely conforms with $1.5\mathcal{S}^{-0.5}$ and the $|a|$ distributions are always well-approximated by Gaussians. When the LT torque is included, only the small-$\mathcal{S}$ models show deviations from Gaussian. In most other cases (with $\mathcal{S} \gtrsim 100$), the random walk impedes the spin down with $a_{RW} \gg a_{crit}$ such that contribution from the LT torque is negligible in the EBH context. This random walk factor have been overlooked in previous analysis of chaotic spin accretion of SMBHs with much larger black hole masses and smaller relevant $\mathcal{S}$ (see Method). We confirm that in the SMBH context, the LT torque can significantly modify the value of $\sqrt{\langle a^2 \rangle}$ and the $a, |a|$ distribution, which could significantly deviate from Gaussian (Figure 1 [Extended Data]) with a deficit in small values[34,35].

We extrapolate the above analysis for stand-alone EBHs to the merging BBHs observed by LIGO-Virgo. If these BBHs form with very close separation and evolve quickly towards coalescence (before the components' spins are significantly modified by three-body encounters and/or multiple-disk interaction), the relative contribution of each member to the merger's $\chi_{\rm eff}$ generally cannot exceed the magnitude of $a_{\rm RW}$ of stand-alone EBHs (see Methods, last section). In widely separated BBHs, the individuals' spins and the BBHs' orbital angular momentum may still have ample time to evolve and couple as they accret prior to merger. But, if they are surrounded by CSDs with persistent spin orientation, non-negligible quadruple moment in the gravitational potential would induce precession in their orbits. Moreover, either BBHs' migration through the global disk or their orbital contraction can lead to eccentricity and inclination excitation through evection and eviction resonances. These effects significantly reduce the magnitude and reorient the direction of BBHs' orbital angular momentum[30]. Although these resonances might otherwise be suppressed for those BBHs embedded in CSD with frequent stochastic spin

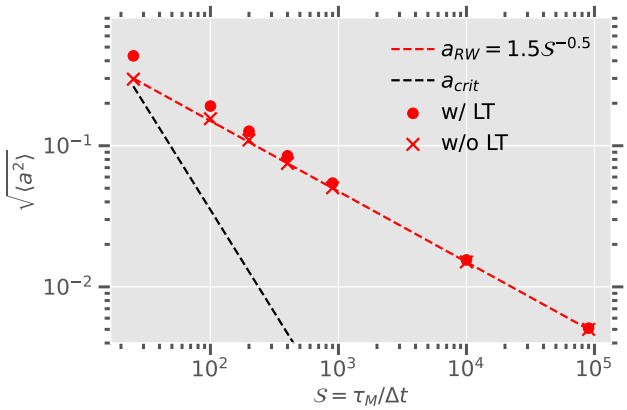

Figure 3. Red dots: The steady-state root mean square spin value of EBH populations after $3\tau_M$ of evolution, varying the spin-reorientation number $\mathcal{S}$. a_{RW} as a function of $\mathcal{S}$ is shown in red dashed line and a_{crit} in black dashed line. For large $\mathcal{S}$ and $a_{crit} \ll a_{RW}$ we verify that the dispersion converges to a_{RW}, and the $|a|$ histograms are consistently Gaussian. when a_{crit}, a_{RW} becomes comparable, the final dispersion begins to deviate from a_{RW} due to LT effects. Nevertheless, $\mathcal{S} \lesssim 100$ is highly unrealistic for the dynamical timescale of disk turbulence and EBH masses.

re-orientation ($\mathcal{S} \gg 1$), the cumulative consequence of accretion on the individual components' spins would be analogous to that of the stand-alone EBHs with asymptotic $\sqrt{\langle a^2 \rangle} \sim a_{\rm RW}$, which sets an upper limit to $\chi_{\rm eff}$. An uncertainty in our model is the assumption that that the turbulence field in the circum-SMBH is able to rapidly change the circumstellar flow over an eddy-turnover timescale. This assumption can be quantitatively tested with follow-up numerical simulations.

During coalescence of EBHs which might contribute to some of the gravitational wave events detected by LIGO, the EBH mass would increase monotonically with resulting $|a| \sim \mathcal{O}(1)$[26]. Such growth may account for EBHs' larger masses in comparison with the BHs in Galactic binary systems, but in order to reconcile with the low-$\chi_{\rm eff}$ found by LIGO, the coalesced EBHs need to substantially reduce their $|a|$ prior to succeeding coalescence with other EBHs and/or randomize their spin axes. To achieve this, we suggest that EBHs' accretion of GI or MRI-induced turbulent gas in the circum-SMBH disks can lead to both mass increases and $|a|$ decreases.

The highly uncertain EBHs' merger timescale $\tau_{\rm merger}$ is determined by many effects including EBHs' migration, mass growth and BBHs' orbital evolution under the influence of circum-BBH disks[36–38] and external secular perturbations[30]. The efficiency of these competing mechanisms are beyond the scope of this letter, but we generally conclude that EBHs' mass increase may be primarily due to mergers/gas accretion in the limit $\tau_{\rm merger} \lesssim \tau_{\rm M} = \tau_{\rm Sal}\eta_\star$. The latter effect of diminishing $|a|$ is due to the ceaseless re-orientation of the relative angle between the EBHs' spin axis and the angular momentum of the turbulent gas accreted onto them. Considering the spin-down and RW-dominated phase of EBH spin evolution through gas accretion, in the limit $\tau_{\rm merge} \gtrsim \tau_{\rm M}$, the first phase takes about time $\tau_d = \tau_{\rm M} \ln\mathcal{S}/5.752 \sim \tau_{\rm M}$ to erase any initial spin and the subsequent evolution is dominated by random motion, until the dispersion reaches an asymptotic value $a_{RW} \sim \mathcal{S}^{-1/2}$ throughout the AGN duration. The gas-accretion contribution would lead to the small $\chi_{\rm eff}(< 0.1)$ reported by the LIGO detection as well as a significant fraction of EBHs' mass growth. In the limit $\tau_{\rm merge} \lesssim \tau_{\rm M}$ when merger is very frequent, the first spin-down phase can not be completed and the lowest reachable value for the characteristic spin is $\sqrt{\langle a^2 \rangle} \sim \exp[-2.876\tau_{\rm merge}/\tau_{\rm M}]$ before merger resets a to $\mathcal{O}(1)$.

We conclude that spin-reorientation of CSDs,fed by rapidly-varying turbulent global disk reconciles efficient gas accretion of EBHs with their low spins, and reinforces the scenario that AGN disks are fertile hosting venues for BBH mergers. Furthermore, a low $\chi_{\rm eff}$ distribution from observation suggests that EBHs' mass growth is dominated by gas accretion rather than their coalescence and the energy dissipated during this process provides intense auxiliary heating sources for the global disk.

Methods

Evolution of BH Spin Parameter

In gaseous disks around SMBHs, accretion onto the EBHs is likely constrained by the Eddington limit $\dot{M}_\star = L_E/\eta_\star c^2$, where the EBH luminosity reaches its Eddington luminosity $L = L_{\rm E} = 1.25 \times 10^{38} M_\star/M_\odot {\rm erg\ s^{-1}}$, and $\eta_\star$ is the efficiency factor of

EBH accretion. The EBH's mass-growth timescale is

$$\tau_{\rm M} \approx \frac{M_\star}{\dot{M}_\star} \simeq \eta_\star \tau_{\rm Sal} \tag{1}$$

where $\tau_{\rm Sal} = M_\star c^2/L_{\rm E} = 4.5\times10^8$ yr is the Salpeter[33] timescale. Within an order-of-magnitude, gas in the circumstellar disks (CSDs) is accreted onto the EBHs at the innermost stable circular orbit (ISCO) $\sim R_{\rm isco}$ with specific angular momentum $j(R_{\rm isco}) \sim \sqrt{GM_\star R_{\rm isco}}$, such that in a quiescent environment the spin parameter $|a|$ evolves towards unity on a similar timescale as τ_M (e.g. Figure 1, black line).

The accretion efficiency $\eta_\star$, which also depends on black hole mass and spin, is usually on the order of a few percent for isolated black holes[39,40] or even lower due to the strong outflow/jet for the EBHs in AGN disks[41,42], which may provide an important source of heating to the global disk environment. Here we neglect feedback effects and assume $\eta_\star$ to be a constant such that τ_M can be a natural unit in our calculations, and $M_\star(t) = M(t=0)\exp(t/\tau_M)$ is a universal mapping of how $M_\star$ evolves with time.

Generally in a turbulent medium, gas accretion occurs in randomly oriented episodes. For SMBH growth over cosmic time, the duration of accretion episodes $\Delta t_\bullet$ may be characterised by the timescale that a total "self-gravitating-disk" mass is accreted at the Eddington rate[34,35]. Alternatively, applied to stellar-mass EBHs in an AGN disk, the episode timescale should be comparable to local dynamical timescale $\Delta t_\star \simeq \Omega^{-1} \ll \tau_M$, which generally reflects the eddy-turnover or auto-correlation time for MRI and gravito-turbulence[43–45]. We consider the appropriate cadence limit such that the number of eddy-spin-reorientation episodes could elapse during one accretion timescale τ_M is

$$\begin{aligned}\mathcal{S} &\equiv \tau_M/\Delta t_\star \simeq \tau_M\Omega \\ &\approx 3\times10^4 \frac{\eta_\star}{0.1}\left(\frac{M_\bullet}{10^8 M_\odot}\right)^{1/2}\left(\frac{D}{\rm pc}\right)^{-3/2}.\end{aligned} \tag{2}$$

Here $M_\bullet$ is the host SMBH mass, and D is the EBH's orbital radius around SMBH. Since the EBH's $\eta_\star$ does not necessarily equal to the *SMBH's* accretion efficiency $\eta_\bullet$, there are $\mathcal{S}\eta_\bullet/\eta_\star$ cycles within the SMBH's growth timescale or the AGN lifetime. But here we consider $\eta_\bullet \sim \eta_\star$ such that the AGN lifetime is comparable to τ_M of individual EBHs.

Given the ratio $\Delta t_\star/\tau_M = \mathcal{S}^{-1}$ as the frequency parameter, we numerically model the evolution of EBH spin as a function of time and mass by the following procedure.

1) During one single continuous accretion episode, starting with an initial black hole mass M_0 and initial a_0, the initial normalized value of $r_{\rm isco} = R_{\rm isco}/R_\star$ can be calculated from the generic relation between $R_{\rm isco}$ and a[23,32,46]:

$$r_{\rm isco} = 3 + Z_2 - {\rm sign}(a)\sqrt{(3-Z_1)(3+Z_1+2Z_2)} \tag{3}$$

$$\begin{aligned} Z_1 &= 1 + \left(1-|a|^2\right)^{1/3}\left[(1+|a|)^{1/3} + (1-|a|)^{1/3}\right] \\ Z_2 &= \sqrt{3|a|^2 + Z_1^2}\end{aligned} \tag{4}$$

The magnitude of $r_{\rm isco}$ ranges from 9 at $a=-1$, to 6 at $a=0$, then ~ 1 as a approaches unity. In the absence of any discontinuous change in the CSD spin direction and $r_{\rm isco}$, the quantity $r_{\rm isco}^{1/2}M_\star = r_{\rm isco,0}^{1/2}M_0$ is conserved[32,34], and a evolves as a mapping of $M_\star$:

$$a(M_\star) = \frac{1}{3}r_{\rm isco,0}^{1/2}\frac{M_0}{M_\star}\left[4 - \left(3r_{\rm isco,0}\left(\frac{M_0}{M_\star}\right)^2 - 2\right)^{1/2}\right] \tag{5}$$

This $a-M_\star$ relation accounts for the fundamental track (Figure 1) in which $r_{\rm isco}$ shrinks 9 times as $M_\star$ grow 3 times from its initial value.

2) In these classical equations, the sign of a is determined by the directions of black hole angular momentum vector $\mathbf{J}_\star$ and local CSD angular momentum $\mathbf{J}_d$ (specific magnitude of which becomes relevant in 3D turbulence), such that $a := |a|{\rm sign}(\mathbf{J}_\star\cdot\mathbf{J}_d)$[23,46]. But if the direction of $\mathbf{J}_d$ of a population of EBHs changes intermittently due to fluctuating turbulence, this definition of a is unimportant in a collective sense. In our formulation, there is an absolute vertical direction $\hat{\mathbf{z}}$ associated with the global SMBH accretion disk's prograde direction, and only the absolute spin $|a|{\rm sign}(\mathbf{J}_\star\cdot\hat{\mathbf{z}})$ may change continuously between switching of EBH accretion cycles, while a alternates between positive and negative values, and $r_{\rm isco}$ changes discontinuously (Eqn. 3) between values larger and smaller than 6.

Evolution of Spin Orientation Due to Turbulence & Lense-Thirring Torque

Simulations suggest that that typical turbulent eddies generated by gravitational[45,47] and magneto-rotational instabilities[48] have length scales $\lesssim H$, where H is the global disk scale height. While magneto-rotational instability is generally isotropic, Gravito-turbulence becomes isotropic on scales $\leq H$, which is larger than the Bondi and Hill radius R_B, R_H of most companion EBHs. For these most common sub-thermal companions with $R_B \lesssim R_H \lesssim H$, or $M_\star/M_\bullet \lesssim h^3$ where $h = H/D$ is the aspect ratio. As a specific example, $M_\star < 100M_\odot$ in environment $h \gtrsim 0.01$ for a $M_\bullet \gtrsim 10^8 M_\odot$ SMBH would be sub-thermal. On this scale where turbulence is isotropic, the dominant eddy that becomes regulated into a CSD by the companion gravity in its vicinity during its lifetime will have a fairly random distribution of average inclination θ with respect to the current BH spin. If the effective disk angular momentum that exerts the LT torque is much smaller than the BH angular momentum, the disk will generally evolve towards alignment with the BH if $\theta < \pi/2$ and counteralignment if $\theta < \pi/2$, on a LT timescale of[49]

$$\tau_{\rm LT} = \frac{J_\star}{J_d/\Delta t} \simeq \frac{|a|GM_\star^2/c}{(L_E/\eta c^2)\sqrt{GM_\star R_{\rm w}}} \simeq \frac{R_\star^{1/2}}{R_{\rm w}^{1/2}}|a|\tau_{\rm M} \tag{6}$$

where the warp radius is given by[49]

$$\begin{aligned}\frac{R_{\rm w}}{R_\star} =& 990\left(\frac{\eta}{0.1}\right)^{1/4}\left(\frac{L}{0.1L_{\rm E}}\right)^{-1/4}\left(\frac{M_\star}{10^8 M_\odot}\right)^{1/8} \\ &\times\left(\frac{\alpha_1}{0.03}\right)^{1/8}\left(\frac{\alpha_2}{0.03}\right)^{-5/8}|a|^{5/8} \\ &\approx 100|a|^{5/8} := r_{w,0}|a|^{5/8}\end{aligned} \tag{7}$$

where α_1, α_2 are the accretion and warp-propagation viscosities. We assume the typical value of $\alpha_1 \sim \alpha_2 \sim 0.03$, and choose $r_{w,0} = 100$ relevant to our EBH parameter $M_\star \sim 10M_\odot$. We also limit $R_w/R_\star > 1$. In our case we have defined $J_d = (\eta L_E/c^2)\sqrt{GM_\star R_{\rm w}}\Delta t_\star$ as the angular momentum that flows past the warp radius[35] during one accretion cycle. Note that $J_d = j(R_w)\dot{M}\Delta t_\star$ is generally much larger than $j(R_{\rm isco})\dot{M}\Delta t_\star$: the former is the total angular momentum responsible for exerting the LT torque, and the latter is only its small fraction that gets directly fed onto the black hole through $R_{\rm isco}$.

When $\Delta t_\star/\tau_M$ is very small or $\mathcal{S}$ is large, generally $J_d \ll J_\star$ and $\tau_{LT} \gg \Delta t_\star$ for moderate values of $|a|$, which means LT torque cannot strongly influence the EBH inclination during any short accretion cycle, and while θ changes randomly between accretion cycles due to jumps in CSD spin axes, the LT effect cannot accumulate in any preferred direction, so the evolution of a is nearly independent of θ. However, $J_d/J_\star \propto |a|^{-11/16}$ increases with a decreasing $|a|$, and $J_d = J_\star$ when $\tau_{LT} = \Delta t_\star$ or $a_{crit} \simeq (R_w(a_{crit})/R_\star)^{1/2}/\mathcal{S}$, which gives

$$a_{crit} \simeq (r_{w,0}/\mathcal{S}^2)^{8/11}. \tag{8}$$

For $|a| \gtrsim a_{crit}$, any initial $\theta > \pi/2$ is generally directed towards π (counter-alignment) by LT torque, but for $|a| \lesssim a_{crit}$, even $\theta > \pi/2$ might be directed towards $\theta = 0$ on a timescale of $\tau_{LT} < \Delta t_*$, which leads to a systematic spin-up of the magnitude of $|a|$ until it fluctuates around the quasi-steady value of $\pm a_{crit}$ [1]. Thus concluded King et al.[34] in their qualitative analysis relevant for SMBHs, but they did not consider influence of the random walk. We demonstrated in Figures 2 & 3 that the distribution of $|a|$ is dominated by random walk when $1/\sqrt{\mathcal{S}} \gg a_{crit}$, but will show later that we can reduce to their scenario when $1/\sqrt{\mathcal{S}} \lesssim a_{crit}$ which is probable for SMBH growth, although unlikely in our context.

In our turbulent models for EBH spin evolution, at the start of every turbulent episode, we pick the initial inclination of $\mathbf{J}_\star$ with respect to $\mathbf{J_d}$ from a uniform isotropic distribution, equivalent to picking $\cos(\theta)$ from a uniform distribution from -1 to 1. If $\cos(\theta)$ has changed sign compared to the previous cycle, a would also change sign and we discontinuously update $r_{\rm isco}$ with Eqn 3, and then evolve a, $r_{\rm isco}$ continuously again with Eqn 5 (replacing $r_{\rm isco,0}^{1/2}M_0$ with the updated $r_{\rm isco}^{1/2}M_\star$), until $\cos(\theta)$ changes sign again either due to LT or continuous spin accretion. The short-term continuous local evolution of θ during every accretion timescale of Δt can be calculated by[49],

$$\frac{d}{dt}\cos\theta \approx \frac{1}{\tau_{\rm LT}J_{BH}}\sin^2\theta(J_d + J_{BH}\cos\theta) \tag{9}$$

where $\tau_{\rm LT}$ is used as a normalization for the dissipation term. Note that $\tau_{\rm LT}$ is only an estimate of the alignment timescale for moderate values of θ, when $\theta \approx \pi$ the actual timescale becomes much larger than τ_{LT} and approaches infinity at $\theta = \pi$ even if $J_{\rm BH} \ll J_d/2$ since there is no LT precession.

[1] The exact long-term alignment criterion is $-2J_{\rm BH}\cos(\theta) < J_d$[49], therefore technically $J_{\rm BH} < J_d/2$ is needed to guarantee systematic spin-up for any random θ, but extra order-unity factors do not qualitatively affect our argument

When $\theta < \pi/2$, the time derivative of $\cos(\theta)$ is always larger than 0 and θ decreases towards 0 ($|a|$ consistently spins up). When $\theta > \pi/2$, however, it is worth clarifying that the long-term evolution of θ is not immediately obvious from its local evolution. For example, if $J_{BH} > J_d$ and $\theta \gtrsim \pi/2$ we should have long term counteralignment, but if the initial $\cos(\theta)$ during this cycle is infinitely close to zero or more generally roughly corresponds to a range of $-J_d/J_\star \lesssim \cos\theta \lesssim 0$, its derivative is actually positive, which would momentarily align the BH with the disk ($|a|$ spins up momentarily). When that happens, we also update a and $r_{\rm isco}$ discontinuously *during* an accretion cycle before applying Equation 5. This prescription does not contradict the long-term counter-alignment criterion since over a longer timescale $\sim \tau_{LT}$ the EBH would eventually tilt back to become counter-aligned with J_d on timescales comparable to τ_{LT}, see Figure 2 of King et al.[49]. However, practically when $\Delta t_\star < \tau_{LT}$, the EBH may not be able to counter-align again before another *new* accretion cycle kicks in and $\cos(\theta)$ is randomized again, so the spin-down is indeed changed to spin-up midway through an accretion cycle even when $J_{BH} > J_d$ in these "lucky" cases. In the "lucky" cases, the EBH spin is momentarily aligned with the disk, then may not grow back towards long-term counter-alignment before the next accretion cycle cuts in.

Nevertheless, our result shows that $|a|$ still relaxes towards typical values around $a_{RW} = 1.5\mathcal{S}^{-1/2}$, and on average $|a|$ never gets below $a_{crit} \ll a_{RW}$ for LT torque to have a strong effect and for the eternal-alignment criterion to play a role. This is because the "lucky" cases roughly corresponds to a range of $-J_d/J_\star \lesssim \cos\theta \lesssim 0$, the chance of which happening for isotropic $-1 < \cos\theta < 1$ during every accretion episode is on the order of

$$\left(\frac{J_d}{J_\star}\right) \sim \left(\frac{a_{crit}}{|a|}\right)^{11/16}, \tag{10}$$

which self-consistently is much smaller than order-unity when $|a|$ stabilizes around the the random walk equilibrium $a_{RW} = 1.5\mathcal{S}^{-1/2} \gg a_{crit}$, and the general evolution of $|a|$ still turns out to be random-walk dominated.

By comparing a_{RW} with Eqn 8 which shows a_{crit} as a steeper power law of $\mathcal{S}$, we have

$$\frac{a_{crit}}{a_{RW}} \approx 20\left(\frac{r_{w,0}}{10^2}\right)^{8/11}\mathcal{S}^{-21/22}. \tag{11}$$

This equation implies that when $r_{w,0} \gtrsim 100$ and $\mathcal{S} \lesssim 20$, a_{crit} may still become larger than a_{RW}, as shown in Figure 3. But this range of $\mathcal{S}$ is too small to be relevant in the current context, i.e. $\Delta t_\star \simeq \Omega^{-1}$.

The Population Model, with and without Lense Thirring Effect

In the population models, given the re-orientation parameter $\mathcal{S}$, the spin of 10^3 EBHs are evolved over a timescale of $3\tau_M$, with each initial spin a_0 sampled from a uniform initial distribution from -1 to 1. The initial orientation is also randomly chosen. The initial mass function is irrelevant to the spin evolution in our setup.

To illustrate the relative importance of LT torque, we also run population evolution of EBHs without LT effect, in which we randomly update $\cos(\theta)$ at the beginning of each spin-reorientation episode but do not allow it to evolve. The physical meaning of these models may be more relevant to super-thermal companions with $R_B \gtrsim R_H \gtrsim H$ or $M_\star/M_\bullet \gtrsim h^3$, like intermediate mass EBHs[20]. The averaged flow within $R_H, R_B > H$, which regulates the rotation of the CSD, may have a 2D nature (at least for gravito-turbulence[45]) and prefer to be co-planar to the midplane of the global disk. Since the vertical flows cancel out, the CSD spin can be on average either completely aligned with the absolute vertical direction or completely counter-aligned during every typical eddy-turnover timescale. In such cases we may neglect the evolution of EBH obliquity due to the Lense-Thirring precessions since any possible initial spin would be directed towards $\theta = 0$ or π and not subject to significant LT torque influence anymore. Nevertheless, in the relevant parameter space, this case is expected to be totally dominated by random walk (Figure 3, red crosses) and not much different from the full turbulence model.

The SMBH Context

As a sanity-check, we show that LT torque may still play a large role when a large $r_{w,0}$ relaxes the viable range of $\mathcal{S}$ for $a_{crit} > a_{RW}$, conforming with previous numerical simulations of SMBH growth[35], first qualitatively suggested in King & Pringle[34]. Considering the central SMBH mass $M_\bullet \sim 10^8 M_\odot$, we can choose $r_{w,0} = 1000$ which is an order of magnitude larger than that in the EBH context. The accretion timescale of King et al.[35] is defined in terms of the self-gravitational disk mass $\tau_{sg} \sim 0.01\tau_M$, which is similar to $\mathcal{S} \simeq 10^2$. For these parameters, we confirm that $a_{crit} > a_{RW}$. The corresponding a histogram for a population of 10^3 SMBHs after $3\tau_M$ of evolution is shown in Figure 1 [Extended Data]. In this case, the systematic spin-up by LT torque can prevent any spin-down below $|a| < a_{crit}$, and clear out a central deficit in the distribution function. The spin parameters are strongly peaked around values comparable to a_{crit}, corresponding to equal spin-up and spin-down efficiency[35].

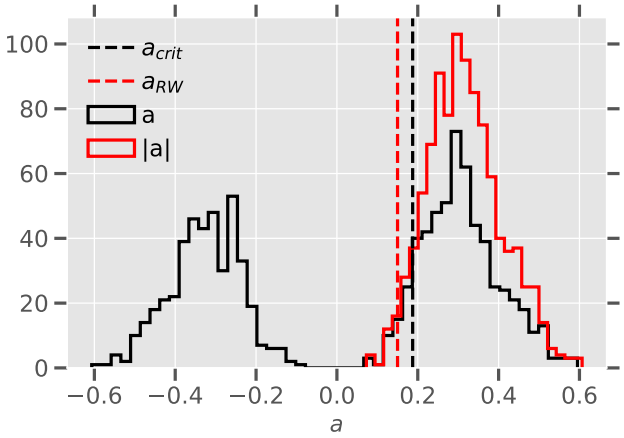

Figure 1. [Extended Data] The semi-steady distribution of a and $|a|$ after 3 τ_M of evolution for the SMBH context, with $r_{w,0} = 1000, \mathcal{S} = 100$. The distribution of $|a|$ can no longer be approximated by Gaussian, but is strongly peaked around values close to a_{crit} (dashed black line), which is already dominating the random walk factor (red dashed line), since systematic spin-up by LT torque can clear out a deficit for any $|a| < a_{crit}$. It can be compared to Figure 4 of King et al.[35].

Nevertheless, we emphasize again that this skewed distribution is hard to achieve in our EBH context unless α_2 is very small, especially when $\alpha_2/\alpha_1 = 2\left(1+7\alpha_1^2\right)/\left[\alpha_1^2\left(4+\alpha_1^2\right)\right]$ is usually much larger than order unity[50]. We conclude that in most of the stellar-mass EBH cases RW would dominate, in the sense when $a_{RW} \gg a_{crit}$, the deficit for $|a| < a_{crit}$, although it exists, is negligible in the entire Gaussian distribution.

Relevance to BBH Mergers and $\chi_{\rm eff}$ Distributions

The detailed influence of an isotropic low-spin distribution on $\chi_{\rm eff}$ needs to be understood through population synthesis incorporating mass functions and more detailed physical effects. Nevertheless, we can offer some natural argument asserting that it's difficult for $\chi_{\rm eff}$ to reach values much larger than a_{RW}. Once captured into BBHs and after binary inspiral, each individual EBH with mass M_1 and M_2 makes a fractional contribution to $\chi_{\rm eff}$, such that

$$\chi_{\rm eff} = \frac{M_1}{M_1+M_2}\chi_1 + \frac{M_2}{M_1+M_2}\chi_2, \qquad \chi_i = |a_i|\cos\psi_i, \qquad i = 1,2 \tag{12}$$

where ψ_i is angle between EBH spin and binary orbital axis. Avoiding making any specific assumptions about the mass distribution, we understand that in the limit that the evolution towards merger is short, we can draw the magnitude of $|a|$ from the positive part of a Gaussian distribution $f(|a|)$, and $\lambda = \cos\psi$ from a uniform distribution $g(\lambda)$ since the spins have yet to couple with the orbital angular momentum. Neglecting all normalization coefficients, we have the cumulative probability distribution (CDF) for positive $\chi = |a|\lambda$ being

$$CDF(0<\chi<|a|\lambda) \propto \int_\chi^1 f(|a|)da \int_{\chi/|a|}^1 g(\lambda)d\lambda \propto \int_\chi^1 f(|a|)\left(1-\frac{\chi}{|a|}\right)da \tag{13}$$

Substituting the exact form of $f(|a|)$, we can derive the probability distribution (PDF) of χ by differentiating the CDF

$$PDF(\chi) \propto -\frac{d}{d\chi}\int_\chi^1 f(|a|)\left(1-\frac{\chi}{|a|}\right)d|a| = \frac{d}{d\chi}\int_\chi^1 f(|a|)\left(\frac{\chi}{|a|}\right)d|a| \approx \int_\chi^\infty \exp\left(\frac{-|a|^2}{2a_{RW}^2}\right)\frac{d|a|}{|a|} \propto \mathcal{E}\left(\frac{\chi^2}{2a_{RW}^2}\right), \tag{14}$$

$$\mathcal{E}(z) := \int_1^\infty \frac{e^{-xz}dx}{x} = \int_z^\infty \frac{e^{-x}}{x}dx. \tag{15}$$

Note we have approximated the upper limit to be ∞ since the integral from 1 to infinity is also negligible. Since the $\chi < 0$ distribution is completely symmetric, after normalization we have:

$$PDF(\chi) \approx \frac{1}{2\sqrt{2\pi}a_{RW}}\mathcal{E}(\frac{\chi^2}{2a_{RW}^2}). \quad (16)$$

This distribution function is very narrow and suggests that χ has $\sim 90.6\%$ probability of being between $\pm a_{\rm RW}$. Since for any general EBH mass function, the mass-weighted average $\chi_{\rm eff}$ cannot exceed the value of χ by much, we can constrain the magnitude of $\chi_{\rm eff}$ produced from the turbulence channel to be $\lesssim a_{RW}$ for the decoupled spin-orbit angular momentum scenario.

Data Availability

Relevant codes will be made publicly available upon publication of this manuscript.

References

1. Ghez, A. M. *et al.* The First Measurement of Spectral Lines in a Short-Period Star Bound to the Galaxy's Central Black Hole: A Paradox of Youth. *ApJL* **586**, L127–L131, DOI: 10.1086/374804 (2003). astro-ph/0302299.
2. Lu, J. R. *et al.* A Disk of Young Stars at the Galactic Center as Determined by Individual Stellar Orbits. *ApJ* **690**, 1463–1487, DOI: 10.1088/0004-637X/690/2/1463 (2009). 0808.3818.
3. Bartko, H. *et al.* Evidence for Warped Disks of Young Stars in the Galactic Center. *ApJ* **697**, 1741–1763, DOI: 10.1088/0004-637X/697/2/1741 (2009). 0811.3903.
4. Bartko, H. *et al.* An Extremely Top-Heavy Initial Mass Function in the Galactic Center Stellar Disks. *ApJ* **708**, 834–840, DOI: 10.1088/0004-637X/708/1/834 (2010). 0908.2177.
5. Law-Smith, J., Ramirez-Ruiz, E., Ellison, S. L. & Foley, R. J. Tidal Disruption Event Host Galaxies in the Context of the Local Galaxy Population. *ApJ* **850**, 22, DOI: 10.3847/1538-4357/aa94c7 (2017). 1707.01559.
6. Law-Smith, J. A. P., Coulter, D. A., Guillochon, J., Mockler, B. & Ramirez-Ruiz, E. Stellar Tidal Disruption Events with Abundances and Realistic Structures (STARS): Library of Fallback Rates. *ApJ* **905**, 141, DOI: 10.3847/1538-4357/abc489 (2020). 2007.10996.
7. Mockler, B. & Ramirez-Ruiz, E. An Energy Inventory of Tidal Disruption Events. *ApJ* **906**, 101, DOI: 10.3847/1538-4357/abc955 (2021). 2007.12198.
8. Kormendy, J. & Ho, L. C. Coevolution (Or Not) of Supermassive Black Holes and Host Galaxies. *ARAA* **51**, 511–653, DOI: 10.1146/annurev-astro-082708-101811 (2013). 1304.7762.
9. Artymowicz, P., Lin, D. N. C. & Wampler, E. J. Star Trapping and Metallicity Enrichment in Quasars and Active Galactic Nuclei. *ApJ* **409**, 592, DOI: 10.1086/172690 (1993).
10. Tanaka, H. & Ward, W. R. Three-dimensional Interaction between a Planet and an Isothermal Gaseous Disk. II. Eccentricity Waves and Bending Waves. *ApJ* **602**, 388–395, DOI: 10.1086/380992 (2004).
11. MacLeod, M. & Lin, D. N. C. The Effect of Star-Disk Interactions on Highly Eccentric Stellar Orbits in Active Galactic Nuclei: A Disk Loss Cone and Implications for Stellar Tidal Disruption Events. *ApJ* **889**, 94, DOI: 10.3847/1538-4357/ab64db (2020). 1909.09645.
12. Toomre, A. On the gravitational stability of a disk of stars. *ApJ* **139**, 1217–1238, DOI: 10.1086/147861 (1964).
13. Gammie, C. F. Nonlinear Outcome of Gravitational Instability in Cooling, Gaseous Disks. *ApJ* **553**, 174–183, DOI: 10.1086/320631 (2001). astro-ph/0101501.
14. Goodman, J. Self-gravity and quasi-stellar object discs. *MNRAS* **339**, 937–948, DOI: 10.1046/j.1365-8711.2003.06241.x (2003). astro-ph/0201001.
15. Jiang, Y.-F. & Goodman, J. Star Formation in a Quasar Disk. *ApJ* **730**, 45, DOI: 10.1088/0004-637X/730/1/45 (2011). 1011.3541.
16. Dittmann, A. J. & Miller, M. C. Star formation in accretion discs and SMBH growth. *MNRAS* **493**, 3732–3743, DOI: 10.1093/mnras/staa463 (2020). 1911.08685.
17. Cantiello, M., Jermyn, A. S. & Lin, D. N. C. Stellar Evolution in AGN Disks. *ApJ* **910**, 94, DOI: 10.3847/1538-4357/abdf4f (2021). 2009.03936.
18. Hamann, F. & Ferland, G. Elemental Abundances in Quasistellar Objects: Star Formation and Galactic Nuclear Evolution at High Redshifts. *ARAA* **37**, 487–531, DOI: 10.1146/annurev.astro.37.1.487 (1999). astro-ph/9904223.

19. Hamann, F., Korista, K. T., Ferland, G. J., Warner, C. & Baldwin, J. Metallicities and Abundance Ratios from Quasar Broad Emission Lines. *ApJ* **564**, 592–603, DOI: 10.1086/324289 (2002). astro-ph/0109006.

20. McKernan, B., Ford, K. E. S., Lyra, W. & Perets, H. B. Intermediate mass black holes in AGN discs - I. Production and growth. *MNRAS* **425**, 460–469, DOI: 10.1111/j.1365-2966.2012.21486.x (2012). 1206.2309.

21. McKernan, B., Ford, K. E. S., Kocsis, B., Lyra, W. & Winter, L. M. Intermediate-mass black holes in AGN discs - II. Model predictions and observational constraints. *MNRAS* **441**, 900–909, DOI: 10.1093/mnras/stu553 (2014). 1403.6433.

22. Bartos, I., Kocsis, B., Haiman, Z. & Márka, S. Rapid and Bright Stellar-mass Binary Black Hole Mergers in Active Galactic Nuclei. *ApJ* **835**, 165, DOI: 10.3847/1538-4357/835/2/165 (2017). 1602.03831.

23. Tagawa, H., Haiman, Z., Bartos, I. & Kocsis, B. Spin Evolution of Stellar-mass Black Hole Binaries in Active Galactic Nuclei. *ApJ* **899**, 26, DOI: 10.3847/1538-4357/aba2cc (2020). 2004.11914.

24. Samsing, J. *et al.* AGN as potential factories for eccentric black hole mergers. **603**, 237–240, DOI: 10.1038/s41586-021-04333-1 (2022).

25. Graham, M. J. *et al.* Candidate Electromagnetic Counterpart to the Binary Black Hole Merger Gravitational-Wave Event S190521g*. *PhRvL* **124**, 251102, DOI: 10.1103/PhysRevLett.124.251102 (2020). 2006.14122.

26. Hofmann, F., Barausse, E. & Rezzolla, L. The Final Spin from Binary Black Holes in Quasi-circular Orbits. *ApJL* **825**, L19, DOI: 10.3847/2041-8205/825/2/L19 (2016). 1605.01938.

27. The LIGO Scientific Collaboration *et al.* GWTC-3: Compact Binary Coalescences Observed by LIGO and Virgo During the Second Part of the Third Observing Run. *arXiv e-prints* arXiv:2111.03606 (2021). 2111.03606.

28. Farr, W. M. *et al.* Distinguishing spin-aligned and isotropic black hole populations with gravitational waves. **548**, 426–429, DOI: 10.1038/nature23453 (2017). 1706.01385.

29. Li, Y.-P., Chen, Y.-X., Lin, D. N. C. & Wang, Z. Spin Evolution of Stellar-mass Black Holes Embedded in AGN Disks: Orbital Eccentricity Produces Retrograde Circumstellar Flows. *ApJL* **928**, L1, DOI: 10.3847/2041-8213/ac5b61 (2022). 2203.05539.

30. Gautham Bhaskar, H., Li, G. & Lin, D. N. C. Blackhole Mergers Through Evection Resonances. *arXiv e-prints* arXiv:2204.07282 (2022). 2204.07282.

31. Balbus, S. A. & Hawley, J. F. Instability, turbulence, and enhanced transport in accretion disks. *Rev. Mod. Phys.* **70**, 1–53, DOI: 10.1103/RevModPhys.70.1 (1998).

32. Bardeen, J. M. Kerr Metric Black Holes. **226**, 64–65, DOI: 10.1038/226064a0 (1970).

33. Salpeter, E. E. Accretion of Interstellar Matter by Massive Objects. *ApJ* **140**, 796–800, DOI: 10.1086/147973 (1964).

34. King, A. R. & Pringle, J. E. Growing supermassive black holes by chaotic accretion. *MNRAS* **373**, L90–L92, DOI: 10.1111/j.1745-3933.2006.00249.x (2006). astro-ph/0609598.

35. King, A. R., Pringle, J. E. & Hofmann, J. A. The evolution of black hole mass and spin in active galactic nuclei. *MNRAS* **385**, 1621–1627, DOI: 10.1111/j.1365-2966.2008.12943.x (2008). 0801.1564.

36. Li, Y.-P., Dempsey, A. M., Li, S., Li, H. & Li, J. Orbital Evolution of Binary Black Holes in Active Galactic Nucleus Disks: A Disk Channel for Binary Black Hole Mergers? *ApJ* **911**, 124, DOI: 10.3847/1538-4357/abed48 (2021). 2101.09406.

37. Li, Y.-P., Dempsey, A. M., Li, H., Li, S. & Li, J. Hot Circumsingle Disks Drive Binary Black Hole Mergers in Active Galactic Nucleus Disks. *arXiv e-prints* arXiv:2112.11057 (2021). 2112.11057.

38. Li, R. & Lai, D. Hydrodynamical Evolution of Black-Hole Binaries Embedded in AGN Discs. *arXiv e-prints* arXiv:2202.07633 (2022). 2202.07633.

39. Jiang, Y.-F., Stone, J. M. & Davis, S. W. A Global Three-dimensional Radiation Magneto-hydrodynamic Simulation of Super-Eddington Accretion Disks. *ApJ* **796**, 106, DOI: 10.1088/0004-637X/796/2/106 (2014). 1410.0678.

40. Jiang, Y.-F., Blaes, O., Stone, J. M. & Davis, S. W. Global Radiation Magnetohydrodynamic Simulations of sub-Eddington Accretion Disks around Supermassive Black Holes. *ApJ* **885**, 144, DOI: 10.3847/1538-4357/ab4a00 (2019). 1904.01674.

41. Pan, Z. & Yang, H. Supercritical Accretion of Stellar-mass Compact Objects in Active Galactic Nuclei. *ApJ* **923**, 173, DOI: 10.3847/1538-4357/ac249c (2021). 2108.00267.

42. Tagawa, H. *et al.* Can Stellar-mass Black Hole Growth Disrupt Disks of Active Galactic Nuclei? The Role of Mechanical Feedback. *ApJ* **927**, 41, DOI: 10.3847/1538-4357/ac45f8 (2022). 2112.01544.

43. Oishi, J. S., Mac Low, M.-M. & Menou, K. Turbulent Torques on Protoplanets in a Dead Zone. *ApJ* **670**, 805–819, DOI: 10.1086/521781 (2007). astro-ph/0702549.

44. Baruteau, C. & Lin, D. N. C. Protoplanetary Migration in Turbulent Isothermal Disks. *ApJ* **709**, 759–773, DOI: 10.1088/0004-637X/709/2/759 (2010). 0912.0964.

45. Booth, R. A. & Clarke, C. J. Characterizing gravito-turbulence in 3D: turbulent properties and stability against fragmentation. *MNRAS* **483**, 3718–3729, DOI: 10.1093/mnras/sty3340 (2019). 1812.05644.

46. Reynolds, C. S. Observational Constraints on Black Hole Spin. *ARAA* **59**, DOI: 10.1146/annurev-astro-112420-035022 (2021). 2011.08948.

47. Riols, A., Latter, H. & Paardekooper, S. J. Gravitoturbulence and the excitation of small-scale parametric instability in astrophysical discs. *MNRAS* **471**, 317–336, DOI: 10.1093/mnras/stx1548 (2017). 1706.06537.

48. Beckwith, K., Armitage, P. J. & Simon, J. B. Turbulence in global simulations of magnetized thin accretion discs. *MNRAS* **416**, 361–382, DOI: 10.1111/j.1365-2966.2011.19043.x (2011). 1105.1789.

49. King, A. R., Lubow, S. H., Ogilvie, G. I. & Pringle, J. E. Aligning spinning black holes and accretion discs. *MNRAS* **363**, 49–56, DOI: 10.1111/j.1365-2966.2005.09378.x (2005). astro-ph/0507098.

50. Ogilvie, G. I. The non-linear fluid dynamics of a warped accretion disc. *MNRAS* **304**, 557–578, DOI: 10.1046/j.1365-8711.1999.02340.x (1999). astro-ph/9812073.

Acknowledgements

We thank Gongjie Li, Hongping Deng and Wenrui Xu for useful conversations.

Author contributions statement

DNCL initiated the project and formulated the conceptual approach with YXC, who carried out the simulations and data analyses. Together they composed the manuscript.

Competing interests

The authors declare no competing interests.

Additional information

Appendix

Analytic approximation of initial spin decay

To approximate the mean decay of spin magnitude, we consider an ideal "alternating model" where the CSD spin flips direction every small fraction of the growth timescale $\Delta t = \tau_M/\mathcal{S}$ with respect to BH spin, and a switches deterministically between positive and negative values. These flips prevent the magnitude of the EBH spin from increasing monotonically towards $|a| \approx 1$, as in a basic accretion cycle. Instead, we can make a fluctuate around zero without introducing RW diffusion factors. We define

$$r_{\rm isco,\pm} = 3 + Z_2 \pm \sqrt{(3-Z_1)(3+Z_1+2Z_2)} \gtrsim 6 \tag{17}$$

respectively on the spin-down (+) and spin-up (-) branches, so that we do not need to involve sign() in taking derivatives. Z_1, Z_2 are defined in Eqn 4.

Consider two cycles starting from black hole mass $M_\star$ and spin a, each cycle accreting a small amount of material approximately $\Delta M = M_\star \Delta t/\tau_M$, on average a small amount will be chiseled off $|a|$ because spin down is a little more efficient than spin up. When $\mathcal{S}$ is large, the sign of vector $\mathbf{J}_\star$ is not changed between two small cycles so the switch of $\mathbf{J_d}$ w.r.t. vertical direction is indistinguishable from that w.r.t. $\mathbf{J}_\star$. As an example, take the first accretion cycle to be spinning down ($a < 0$ regardless of a_{abs}), so we should adopt $r_{\rm isco+}$ to calculate the reference isco radius:

$$\Delta a_1 = M_\star \frac{\Delta t}{\tau_M} \left.\frac{da}{dM_\star}\right|^{M_0=M_\star}_{r_{\rm isco,0}=r_{\rm isco+}(a)}, \tag{18}$$

After EBH's spin w.r.t CSD grew to be $a+\Delta a_1$, but then the CSD flips so w.r.t CSD the EBH spin parameter becomes $-a-\Delta a_1$, and in this adjacent spin up phase the EBH gains

$$\Delta a_2 = [M_\star + \Delta M]\frac{\Delta t}{\tau_M}\frac{da}{dM_\star}\Big|^{M_0=M_\star+\Delta M}_{r_{\rm isco,0}=r_{\rm isco-}(a+\Delta a_1)}. \tag{19}$$

After two cycles, the CSD spin switches again and a becomes $a+\Delta a_1-\Delta a_2$. To first order, Δa_1 and Δa_2 scale linearly with Δt since

$$\frac{da}{dM_\star}\Big|^{M_0=M_\star+\Delta M}_{r_{\rm isco,0}=r_{\rm isco,\pm}(a+\Delta a_1)} = \frac{da}{dM_\star}\Big|^{M_0=M_\star}_{r_{\rm isco,0}=r_{\rm isco,\pm}(a)} + \mathcal{O}(\Delta t). \tag{20}$$

Neglecting small terms, since the above equations should be first order, we have from Eqn 5 that

$$\frac{da}{dM_\star}\Big|^{M_0=M_\star(t)}_{r_{\rm isco,0}=r_{\rm isco,\pm}(a)} = \frac{1}{M_\star}\left(\frac{r_{\rm isco,\pm}(a)^{3/2}}{(3r_{\rm isco,\pm}(a)-2)^{1/2}} - r_{\rm isco,\pm}(a)^{1/2}[4-(3r_{\rm isco,\pm}(a)-2)^{1/2}]\right) := \frac{\mathcal{F}_\pm(a)}{M_\star}. \tag{21}$$

The net change in a during a spin-up followed by a spin-down event becomes

$$\Delta a = \Delta a_1 - \Delta a_2 = [\mathcal{F}_+(a)-\mathcal{F}_-(a)]\Delta t/\tau_M. \tag{22}$$

For $a=0$, $[\mathcal{F}_+(a)-\mathcal{F}_-(a)]=0$ and in the limit $|a|\ll 1$,

$$[\mathcal{F}_+(a)-\mathcal{F}_-(a)] = \frac{d[\mathcal{F}_+(a)-\mathcal{F}_-(a)]}{da}\Big|_{a=0} a + \mathcal{O}(a^2) = -5.752a + \mathcal{O}(a^2). \tag{23}$$

which implies that the rate of change for a on average is

$$\frac{\Delta a}{2\Delta t} \approx -2.876a/\tau_M, \tag{24}$$

When $\Delta t\to 0$ at $\mathcal{S}=\infty$, the asymptotic limit for a evolution in the alternating case is to alternate between $\pm|a_0|e^{-2.876t/\tau_M}$, while $|a|$ monotonically decreases. Although Eqn 23 is valid in the limit of small $|a|$, the exponential function can approximate the entire evolution very well since the initial decay of $|a|$ is quite rapid (See Figure 1, green dotted line). The decay time can be calculated as $\tau_d \approx \tau_M \ln\mathcal{S}/5.752$, which is the time for $|a_0|=1$ to reach $|a|=\mathcal{S}^{-0.5}$, while for other values of initial $|a_0|$ the decay time is even shorter. One may also introduce a shortening of $-0.14\tau_M$ in τ_d for reaching the more accurate converged value $a_{RW}=1.5\mathcal{S}^{-0.5}$ (Figure 2) instead of $\mathcal{S}^{-0.5}$, which is not significant. On a population level, τ_d marks the transition of an initial average spin-down phase towards the steady-state dominated by RW.